
Jacobian Determinant of Normalizing Flows

Huadong Liao Jiawei He

Abstract

Normalizing flows learn a diffeomorphic mapping between the target and base distribution, while the Jacobian determinant of that mapping forms another real-valued function. In this paper, we show that the Jacobian determinant mapping is unique for the given distributions, hence the likelihood objective of flows has a unique global optimum. In particular, the likelihood for a class of flows is explicitly expressed by the eigenvalues of the auto-correlation matrix of individual data point, and independent of the parameterization of neural network, which provides a theoretical optimal value of likelihood objective and relates to probabilistic PCA. Additionally, Jacobian determinant is a measure of local volume change and is maximized when MLE is used for optimization. To stabilize normalizing flows training, it is required to maintain a balance between the expansiveness and contraction of volume, meaning Lipschitz constraint on the diffeomorphic mapping and its inverse. With these theoretical results, several principles of designing normalizing flow were proposed. And numerical experiments on high-dimensional datasets (such as CelebA-HQ 1024²) were conducted to show the improved stability of training.

1. Introduction

Density estimation is a core paradigm in machine learning that aims to learn the underlying representation of data distribution, mathematically, to estimate an unobservable probability density $p_{\mathbf{X}}$ based on an i.i.d. dataset $\mathbf{D} = \{\mathbf{x}^{(n)}\}_{n=1}^N$ drawn from that distribution. This task is challenging in real world applications, since feature \mathbf{x} is usually high-dimensional and complex, thus one can not parameterize $p_{\mathbf{X}}$ directly. Recently, an attractive solution to this task, called normalizing flows, has gained great popularity for its efficient and exact evaluation on inference and sampling, and

Correspondence to: Huadong Liao <natur-omics.liao@gmail.com>.

Preliminary work.

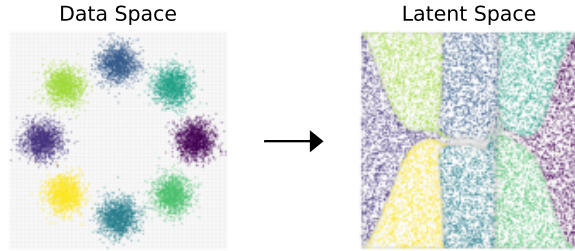


Figure 1. Normalizing flows are diffeomorphic maps and able to provide topology-preserving latent representations, where the latent is uniformly distributed on the same domain as the data space.

useful latent representation for downstream tasks (Fig. 1). More specifically, normalizing flows are derived from the change of variables theorem, estimating probability density by leveraging a sequence of diffeomorphic mappings $\mathbf{g}_{\theta} = \mathbf{g}_1 \circ \mathbf{g}_2 \circ \dots \circ \mathbf{g}_L : \mathbb{R}^d \rightarrow \mathbb{R}^d$ with inverse $\mathbf{f} = \mathbf{g}^{-1}$. Here $\theta = \{\theta_1, \theta_2, \dots, \theta_L\}$ is the parameters of \mathbf{g} and the latent representation $\mathbf{z} = \mathbf{f}(\mathbf{x})$ is assumed to follow a distribution with known form probability density $q_{\mathbf{Z}}$. Given by the theorem, the likelihood for a point \mathbf{x} can be obtained by

$$\begin{aligned} p(\mathbf{x}) &= q(\mathbf{f}(\mathbf{x})) |\det(J_{\mathbf{f}}(\mathbf{x}))| \\ &= q(\mathbf{f}(\mathbf{x})) \prod_{l=1}^L |\det(J_{\mathbf{f}_l}(\mathbf{h}_l))|, \end{aligned} \quad (1)$$

where $J_{\mathbf{f}}(\mathbf{x}) := \partial \mathbf{f}(\mathbf{x}) / \partial \mathbf{x}$ is the Jacobian of \mathbf{f} w.r.t \mathbf{x} , $\det(\cdot)$ denotes the determinant, and \mathbf{h}_l denotes the output of intermediate mapping \mathbf{g}_l , with $\mathbf{h}_1 = \mathbf{x}$ and $\mathbf{h}_L = \mathbf{g}_L(\mathbf{z})$. Given the observed dataset \mathbf{D} , the parameters θ can be learned using statistical technique such as maximum likelihood estimation (MLE):

$$\theta^* = \arg \max_{\theta} \mathcal{L}, \quad \mathcal{L}(\theta; \mathbf{D}) = \sum_{n=1}^N \log p_{\theta}(\mathbf{x}^{(n)}). \quad (2)$$

Theoretically, normalizing flow is powerful to learn probability distribution with arbitrary complexity, supposing the mapping \mathbf{g} is expressive enough. But in practice, there is an obstacle posed by the computation of determinant term, since it has a cubic cost in the dimension of the Jacobian matrix.

To address this computational challenge, at least three strategies have been investigated in the machine learning community. A first approach involves the application of the matrix determinant lemma (Rezende & Mohamed, 2015; van den Berg et al., 2018), which converts the calculation of Jacobian determinant into the determinant of a lower rank matrix, thus the cost is reduced to the cube of the dimension of the lower rank matrix. A second approach involves the stochastic approximation of log-determinant. Example of this approach is to expand the log-determinant into a power series in terms of the trace of power of Jacobian (Behrmann et al., 2019; Grathwohl et al., 2019; Chen et al., 2019). A third approach involves a basic property in linear algebra that the determinant for matrices in special form is cheap to calculate, e.g., the determinant of triangular or diagonal matrix is simply the product of its diagonal terms, in which case the cost is linear in dimensionality. Partition-based flows, which are further divided into flow-based (Dinh et al., 2014; 2017) and autoregressive models (Kingma et al., 2016; Papamakarios et al., 2017), utilize this property by splitting the input of model into parts and constructing ordered dependencies between parts (i.e. the transform on the i -th part only depends on parts 1 to i), enforcing Jacobian matrix to be triangular. This family is popular due to (1) its exact likelihood, (2) computational tractability, and (3) analytic inverse, while the others lack one or two of these features.

The consequence of restricting determinant is limited expressivity of flows. To make up for this limitation, a main branch of research on flows is to construct more powerful diffeomorphic mapping under the above strategies. Remarkable work within this line includes Glow (Kingma & Dhariwal, 2018), Flow++ (Ho et al., 2019), Augmented Flows (Huang et al., 2020a), ResFlows (Chen et al., 2019), among others. Meanwhile, another branch tries to find out whether these restricted flows are universal for arbitrary distributions in theory (Kong & Chaudhuri, 2020; Teshima et al., 2020; Koehler et al., 2020; Huang et al., 2020b). Moreover, optimal transport theory was introduced to provide different convergence properties from MLE (Zhang et al., 2018; Yang & Karniadakis, 2020; Onken et al., 2020).

Despite these tremendous advances, the property of Jacobian determinant was not well studied in the context of normalizing flows. The Jacobian determinant can be seen as another mapping different from the diffeomorphism, and is a part of optimization objective. From this view, it is natural to ask (i) if the determinant mapping given by flows is unique, (ii) what the relation is between its continuity and convergence, and (iii) how it affects the performance of flows. In this work, we focus on these questions, aiming to provide a better understanding of normalizing flows.

Our contributions are summarized as follows.

- We show the Jacobian determinant mapping of flows

is unique for two given distributions, when there are multiple equivalent diffeomorphisms corresponding to that mapping. In particular, we show the determinant mapping for a class of flows has a closed form, thus a theoretical global optimum of likelihood objective is available. For such flows, the relation to PPCA is further built.

- We present there is an equilibrium between the expansion and contraction of volume. This balance requires bounded determinant, and Lipschitz constraint on the diffeomorphism and its inverse to ensure convergence.
- Based on our theoretical results, we propose a new flow and demonstrate its improved stability on high-resolution natural images (CelebA HQ 1024×1024). In addition, various experiments were performed to explain the dynamics of normalizing flows.

2. Properties of Jacobian Determinant

In this section, we begin by discussing the existence and uniqueness of the solution of normalizing flows, specifically showing the closed form of likelihood objective for a subset of flows and the relation of those flows to Probabilistic Principal Component Analysis (PPCA; Tipping & Bishop 1999). We then analyze the optimization behaviour of normalizing flows, and give out the conditions on robust training.

2.1. Existence and Uniqueness

2.1.1. GENERAL FLOW

Given a measure space $(\Omega, \mathcal{F}, \mu)$, a measurable space (Ω', \mathcal{F}') , and a measurable mapping $g : \Omega \rightarrow \Omega'$, one can define a push-forward measure as $g_{*\mu}(U) = \mu(g^{-1}(U))$, for all $U \in \mathcal{F}'$. For the problem of representation learning or generative modelling (e.g., normalizing flows), one can interpret Ω as a latent space, given a set of samples from a measured "data" space $(\Omega', \mathcal{F}', \nu)$, the task is to find a function g such that $g_{*\mu} = \nu$. The existence of g can be guaranteed by the Radon-Nikodym theorem (Rudin, 1987) when extra conditions satisfied:

Theorem 1. (Radon-Nikodym) *Let μ and ν be two σ -finite measures on the same measurable space (Ω, \mathcal{F}) , if ν is absolutely continuous with respect to μ , then (a) there is an Ω -measurable function $\tau : \Omega \rightarrow [0, \infty)$, such that $\nu(U) = \int_U \tau d\mu$, for all $U \in \mathcal{F}$; (b) such function is unique upto a.e. equality w.r.t. μ .*

The function τ is called Radon-Nikodym derivative, and commonly written as $\tau = \frac{d\nu}{d\mu}$. Mapping g exists and is any function satisfying $g_{*\mu} = \nu$ and $|\det(J_{g^{-1}})| = \tau$. If we further restrict μ and ν to probability measures (i.e., $\mu(\Omega) = \nu(\Omega) = 1$), which is a basic assumption in normalizing

flows literature, then τ corresponds to the determinant term of Eq. (1), or the density ratio $p(\mathbf{x})/q(\mathbf{g}^{-1}(\mathbf{x}))$ between target and base distribution. Using probability terminology, Theorem 1 implies that if two random vectors \mathbf{X} and \mathbf{Z} are on the same sample space, and there is a bijective and absolutely continuous mapping $\mathbf{g} : \mathbf{Z} \rightarrow \mathbf{X}$ (whose inverse is $\mathbf{f} = \mathbf{g}^{-1}$), then *there is a unique mapping $\tau : \mathbf{x} \rightarrow [0, \infty)$ such that $\tau = \frac{p(\mathbf{x})}{q(\mathbf{f}(\mathbf{x}))} = |\det(J_{\mathbf{f}})|$* . Note the uniqueness of τ does not imply the uniqueness of \mathbf{g} , e.g., τ is equivalent between $\mathbf{g} = \mathbf{f}^{-1}$ and $\mathbf{g}' = (\mathbf{Q}\mathbf{f})^{-1}$, for \mathbf{Q} being an arbitrary orthogonal matrix.

In the rest of this paper, if not specified, we assume \mathbf{z} is uniformly distributed in $(0, 1)^d$ (i.e., μ is a Lebesgue measure). Because if $q_{\mathbf{Z}}$ is not uniform, we can always find an additional mapping \mathbf{f}' to transform \mathbf{z} to a uniform and let its Jacobian determinant be exactly the density $q_{\mathbf{Z}}$, so the problem does not change but has a new transform $\mathbf{g} \leftarrow \mathbf{g} \circ \mathbf{f}'^{-1}$, $\mathbf{f} \leftarrow \mathbf{f}' \circ \mathbf{f}$. With this setting, Eq. (1) is simplified to

$$p(\mathbf{x}) = \tau : \mathbf{x} \mapsto |\det(J_{\mathbf{f}}(\mathbf{x}))|. \quad (3)$$

We refer Eq. (3) as Jacobian determinant mapping, \mathbf{f} and \mathbf{g} as diffeomorphic mappings in the next.

2.1.2. QUASI-LINEAR FLOW

We have shown the uniqueness of Jacobian determinant mapping by Radon-Nikodym theorem. Here we further present the detailed form of τ when additional constraint is applied to the diffeomorphic mapping.

Consider normalizing flows in the following special form:

$$\begin{aligned} \mathbf{f}(\mathbf{x}) &= \mathbf{W}(\mathbf{x})\mathbf{x} + \mathbf{b}(\mathbf{x}), \\ \text{s.t. } \mathbf{f} &\sim \mathcal{N}(\mathbf{0}, \mathbf{I}), \det(J_{\mathbf{f}}) = \det(\mathbf{W}), \forall \mathbf{x} \in \mathbf{X}, \end{aligned} \quad (4)$$

where $\mathbf{W}(\mathbf{x}) \in \mathbb{R}^{d \times d}$ and $\mathbf{b}(\mathbf{x}) \in \mathbb{R}^d$ are parameterized by or independent of \mathbf{x} . To simplify the analysis, we omit the bias term $\mathbf{b}(\mathbf{x})$ in the following, as it can be treated as part of $\mathbf{W}(\mathbf{x})$ by adding some constant dimensions to \mathbf{x} (or assuming \mathbf{x} is zero-centered thus bias term is zero). A class of previously proposed flows can be rewritten in this form, including linear mapping (Kingma & Dhariwal, 2018), affine/additive coupling layers (Dinh et al., 2014; 2017), dynamic linear layers (Liao et al., 2019), affine autoregressive flows (Kingma et al., 2016; Papamakarios et al., 2017), and their compositions. We call them Quasi-Linear Flow (QLF), since the formula is similar to a linear function, and it does degenerate to a conventional linear mapping when \mathbf{W} and \mathbf{b} are independent of \mathbf{x} .

For QLF, we have $\tau = \mathcal{N}(\mathbf{f}; \mathbf{0}, \mathbf{I}) \det(\mathbf{W})$, and the corre-

sponding log-likelihood:

$$\mathcal{L} = \mathbb{E}_{p_{\mathbf{X}}} \left[-\frac{1}{2} \left\{ d \log 2\pi + \text{tr}(\mathbf{M}\mathbf{S}) + \log |\det(\mathbf{M}^{-1})| \right\} \right], \quad (5)$$

where $\mathbf{M} = \mathbf{W}(\mathbf{x})^T \mathbf{W}(\mathbf{x})$, and $\mathbf{S} = \mathbf{x}\mathbf{x}^T$ is the auto-correlation matrix of individual data point. The above log-likelihood is maximized when $\mathbf{W}(\mathbf{x}) = \mathbf{U}\mathbf{\Lambda}^{-1/2}\mathbf{V}^T$, in which \mathbf{U} is an arbitrary $d \times d$ orthogonal matrix, and \mathbf{V} is also a $d \times d$ matrix whose columns are the eigenvectors of \mathbf{S} , with $\mathbf{\Lambda} = \text{diag}(\lambda_1, \lambda_2, \dots, \lambda_d)$ the corresponding diagonal matrix of eigenvalues. Substituting the results into \mathcal{L} , the global maximum of the log-likelihood is uniquely given by

$$\mathcal{L}_{\max} = \mathbb{E}_{p_{\mathbf{X}}} \left[-\frac{1}{2} \left\{ d \log(2\pi) + d + \sum_{i=1}^d \log \lambda_i \right\} \right]. \quad (6)$$

The \mathcal{L}_{\max} is independent of the parameters of flow, and available based on the observed dataset. This provides a theoretical optimal value of likelihood objective.

From PPCA to QLF. QLF can be treated as a nonlinear extension of Probabilistic PCA, where PPCA is the case when \mathbf{W} and \mathbf{b} are independent of \mathbf{x} , i.e., globally shared over all points $\mathbf{x} \sim p_{\mathbf{X}}$. As a generalization, QLF describes flows that can be approximated by a set of linear functions locally, and is allowed to stack multi-layers to get a highly complex model. For PPCA, the expectation in Eq. (5) can be moved into the trace operation $\text{tr}(\cdot)$, therefore \mathcal{L}_{\max} is given by the eigenvalues of covariance matrix of dataset (Tipping & Bishop, 1999), instead of auto-correlation matrix of individual sample. PPCA is typically discussed in the context of dimensionality reduction, where the eigenvalues are descending-ordered and the corresponding first r ($r \leq d$) eigenvectors are called principal axes. Normalizing flows does not have the concept of "principal axes", but it inherits many properties of PPCA, e.g., the learned model captures the variance in different direction of data space rather than high level concept such as object semantic, which explains the observation in previous study (Appendix D in Dinh et al. 2017).

2.2. Equilibrium between Expansion and Contraction

As far, we have theoretical guarantees for the existence and uniqueness of flows. However, more conditions are needed for its convergence, particularly when the optimization is calculated using a machine with limited numerical accuracy. For example, the phenomenon of training instability was observed in previous work (Dupont et al., 2019; Meng et al., 2020) and practical applications.¹ In this section, we provide an intuitive understanding of optimization behaviour of flows.

¹For example, <https://github.com/openai/glow/issues/40>.

As we know, the Jacobian determinant is a measure of local volume change given by a differentiable function, and is also approximately proportional to the variance change for points in a small region. Note that the objective of normalizing flows is to maximize likelihood (Eq. (2)), thus plays an expansive effect on volume. If no constraint was applied to the diffeomorphic mapping \mathbf{f} , the determinant τ will constantly increase as the training iterations update, as well as the variance of output of hidden layers, finally leads to the problem of gradient exploding or vanishing. Now consider the basic assumption $\mathbf{f} \sim \mathcal{U}_d(0, 1)$ aforementioned in Sec. 2.1.1, and let $\mathbf{f} = \mathbf{f}_a \circ \mathbf{f}_b$ in which \mathbf{f}_a is the last layer of \mathbf{f} . The last layer \mathbf{f}_a is usually chosen from functions whose range are explicitly bounded in $(0, 1)^d$, e.g., the cumulative distribution function (CDF) of gaussian distribution, thus $\mathbf{f}_b \sim \mathcal{N}(\mathbf{0}, \mathbf{I})$ and

$$\log \tau \propto \log |\det J_{\mathbf{f}_b}| - \frac{1}{2} \mathbf{f}_b^T \mathbf{f}_b. \quad (7)$$

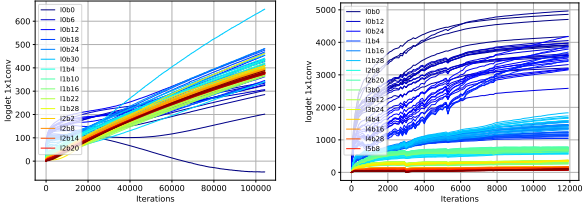
To maximize $\log \tau$, the determinant term in Eq. (7) still plays an expansiveness effect, while the other term plays an anti-effect by encouraging \mathbf{f}_b to be distributed around the origin. This subtle balance is strong enough to guarantee the stability of flows with shallow layers, but as the more layers are stacked, the greater the challenge is to transfer the contraction effect to the early layer by backpropagation.

Fig.2 shows a counterexample based on Glow (Kingma & Dhariwal, 2018). The invertible 1×1 convolution introduced by this study is a linear mapping for permuting the dimensions between two coupling layers, and has shown improvement on performance. However, it is also found unstable after increasing the depth of the model and/or the dimension of input features. The determinant contributed by this module is given by the determinant of convolution weight and independent of input data. The only way to prevent the weight turning to infinity is the contraction regularization by backpropagation, which becomes weak for early layers in a deep model. In a subsequent study by Liao et al. (2019), L_2 regularization was applied to the weight to penalize the unreasonable increase of determinant, and improvement on stability was observed. In the next, we will explain this phenomenon by analyzing the boundedness of Jacobian determinant mapping.

2.3. Conditions on Bounded Gradient

Suppose \mathbf{f} is K -Lipschitz continuous. By the differentiability of \mathbf{f} , we have $\|J_{\mathbf{f}}(\mathbf{x})\| \leq K, \forall \mathbf{x} \in \mathbf{X}$. Furthermore, the Lipschitz constant K is related to Jacobian determinant by Hadamard's inequality:

$$|\det J_{\mathbf{f}}(\mathbf{x})| \leq \prod_{i=1}^d \|J_{\mathbf{f}}(\mathbf{x})\mathbf{e}_i\| \leq \|J_{\mathbf{f}}(\mathbf{x})\|^d \leq K^d, \quad (8)$$



(a) ImageNet 32×32

(b) CelebA 256×256

Figure 2. Training curves of log-determinant for invertible 1×1 convolution in each layer of flow. The value is increasing over iterations as it is maximized by the objective, where the trend is particularly obvious for earlier layers, and the scale is proportional to the dimension of input features ((a) vs. (b)). This result is obtained by training Glow with 256 (vs. 512 in official implementation) hidden units. The legend denotes the order of level and block for each layer.

where \mathbf{e}_i is a unit eigenvector of $J_{\mathbf{f}}(\mathbf{x})$. The Eq. (8) builds a connection between the boundedness of τ and the Lipschitzness of \mathbf{f} , in which the d -power of Lipschitz constant of \mathbf{f} is an upper bound of τ .² For a fixed K , τ has an exact maximum, which is not what we want as our goal is to maximize $\log \tau$. The question is, whether it is reasonable to let K be finite and τ bounded.

We answer this question by analyzing the derivatives of log-likelihood. Since $\nabla_{\theta} \mathbb{E}[\log p(\mathbf{x}; \theta)] = \mathbb{E}[\nabla_{\theta} \log p(\mathbf{x}; \theta)]$, let us consider this score function at a single point, and decompose it as follows:

$$\frac{\partial \log p(\mathbf{x}; \theta)}{\partial \theta} = \left\{ \frac{\partial \log p(\mathbf{x}; \theta)}{\partial \theta_l}, l = 1, 2, \dots, L \right\}. \quad (9)$$

To simplify notations, we denote ∇_{θ_l} and $\nabla_{\mathbf{h}_l}$ the derivatives of $\log p(\mathbf{x})$ w.r.t. θ_l and \mathbf{h}_l , respectively. Given by the chain rule, we have the following recursive formulas:

$$\nabla_{\mathbf{h}_l} = J_{\mathbf{f}_l}^T(\mathbf{h}_l) \nabla_{\mathbf{h}_{l+1}} + \frac{\partial \log |\det J_{\mathbf{f}_l}|}{\partial \mathbf{h}_l}, \quad (10)$$

$$\nabla_{\theta_l} = \frac{\partial \mathbf{h}_{l+1}}{\partial \theta_l^T} \nabla_{\mathbf{h}_{l+1}} + \frac{\partial \log |\det J_{\mathbf{f}_l}|}{\partial \theta_l}, \quad (11)$$

for $1 \leq l \leq L$ and initial condition $\nabla_{\mathbf{h}_{L+1}} = \mathbf{0}$ a zero vector. From Eq. (10) and (11), by the triangle inequality and sub-multiplicativity property of norms, we have

$$\|\nabla_{\theta_l}\| \leq \left\| \frac{\partial \mathbf{h}_{l+1}}{\partial \theta_l} \right\| \|\nabla_{\mathbf{h}_{l+1}}\| + \left\| \frac{\partial \log |\det J_{\mathbf{f}_l}|}{\partial \theta_l} \right\| \quad (12)$$

$$\leq \left\| \frac{\partial \mathbf{h}_{l+1}}{\partial \theta_l} \right\| \cdot \prod_{j=l+1}^L \|J_{\mathbf{f}_j}\| + o, \quad (13)$$

in which $o = o(\|\frac{\partial \mathbf{h}_i}{\partial \theta_i}\|, \|\frac{\partial \log |\det J_{\mathbf{f}_i}|}{\partial \theta_i}\|, \|\frac{\partial \log |\det J_{\mathbf{f}_i}|}{\partial \mathbf{h}_i}\|)$ ($i \geq l$) is a non-negative residual term, and the equality

²Commonly only positive determinant is considered thus also bounded below by zero.

holds under certain conditions. Therefore, we have the following statement.

Proposition 1. (Bounded gradient requires bounded Jacobian determinant) *For $1 \leq l \leq L$, if $\|\nabla_{\theta_l}\|$ is bounded from above by a constant $C > 0$, then there exists a constant $K > 0$ such that $\sum_{j=l+1}^L \log |\det J_{f_j}| \leq d \log K$. Furthermore, each component $|\det J_{f_i}|$ is bounded.*

The proof is straightforward by Eq. (8) and (13). If $\prod_j \|J_{f_j}\|$ is unbounded, $\|\nabla_{\theta_l}\|$ is unbounded, and so as $\sum_j \log \det(J_{f_j})$. See the Appendix for detailed derivation.

By Proposition 1, for a fixed C , when the depth of flow L and the dimension of feature d increase, the Lipschitz constant K_{f_i} for every intermediate mapping f_i should decrease to ensure the gradients of early layers being bounded. This explains the difference between Fig 2(a) and (b), where the log-determinant of higher dimension dataset is significantly larger than the one of lower dimension dataset, and the problem of gradient instability is more common in models for high-dimensional dataset. On the other hand, $|\det J_{f_j}| > 0$ follows from the invertibility of f , so $\det J_{f^{-1}} < K'$ and the inverse f^{-1} is also Lipschitz continuous. The Lipschitzness on f and its inverse guarantees the volume expansion and contraction balance discussed in Sec. 2.2.

3. Principles of Designing Normalizing Flow

In this section, we further discuss normalizing flows from practical aspects.

3.1. Lipschitzness

As a result of the previous section, f is Lipschitz constrained to bound the gradient, but the constant K is flexible to choose. This flexibility brings a trade-off between the expressivity of the mapping and the stability of optimization. Because a tight bound is harmful to the expressivity (by Eq. (8)), while a loose bound may lead to the collapse of optimization (by Proposition 1). One choice of dealing with this trade-off is to explicitly define the constant K as a hyperparameter when constructing model, e.g., use spectral normalization to control the value of K for linear maps (Miyato et al., 2018), and fine-tune the K during training. This is difficult because additional effort is needed and K is not always controllable. Another choice is to limit the variance of the hidden output of model, as its change is approximately proportional to the change of determinant. Methods in this way include (1) using contractive activations those have zero derivative at region far from the origin, such as tanh and normal CDF, (2) adding additional regularization such as L_2 transport cost (Onken et al., 2020), and (3) applying a prior distribution to the parameter of model.

3.2. Blockwise Volume-preserving Initialization

The initialization of flows has non-negligible impact on the convergence. If every layer was initialized as a contraction (an expansion) mapping, after the cumulative effect of multiple layers, the variance of hidden layers may become very small (large), which may slow down or even stop the convergence. A widely used strategy is the volume-preserving initialization, where every layer is initialized to have zero log-determinant, e.g., initializing the weight of linear mapping with identity or orthogonal matrix. We can extend this strategy to blockwise volume-preserving initialization, where in each block an expansion initialization is followed by a contraction initialization, but their combined effect still has zero log-determinant. The idea of this strategy is from our observation that a map with positive log-determinant is usually followed by a map with negative log-determinant in a trained flow (Fig. 4 (c)).

3.3. Multimodality

Let us denote $\sigma(\tau)$ as the number of local maxima of function $\tau : \mathbb{R}^d \rightarrow \mathbb{R}$. We say τ is multimodal if $\sigma(\tau) > 1$ on its domain. With this definition, we can roughly evaluate the complexity of a probability distribution by $\sigma(p(\mathbf{x}))$, and the capacity of a normalizing flow by $\max_{\theta} \sigma(J_{g}(\mathbf{z}; \theta))$. If a target distribution $p(\mathbf{x})$ can be perfectly modeled by a flow $g_{\theta}(\mathbf{z})$, it must satisfy $\sigma(p(\mathbf{x})) \leq \max_{\theta} \sigma(J_{g}(\mathbf{z}; \theta))$. The intuition behind this is, the modes of density function that a flow is able to provide over its parameter space should not be less than the ones of target distribution, or it is impossible for the model to fit the target distribution perfectly. Therefore, to design a powerful flow, aside from increasing the depth of the model, one approach is to improve the capacity of each intermediate layer to provide multimodality. For example, using a mixture of logistics (Ho et al., 2019), or monotonic spline interpolation (Müller et al., 2019; Durkan et al., 2019).

Summarily, normalizing flow can be considered as a sequence of deformations (such as stretching and contraction) between two manifolds, but the distortion at each step is limited so no tearing and gluing appear (the Lipschitz condition). See Fig. 3 for an illustration. For designing a universal flow, the limit exists by improving the capacity of single mapping. But fortunately, the combination of mappings can provide high modality thus breaking the limit.

4. Proposed Flow

To exam our theoretical results, we propose a new flow in this section. Our model is built on the work of RealNVP (Dinh et al., 2017), Glow and NSF (Durkan et al., 2019). The basic block of our model includes three components: (i) a linear layer to enhance the interaction of

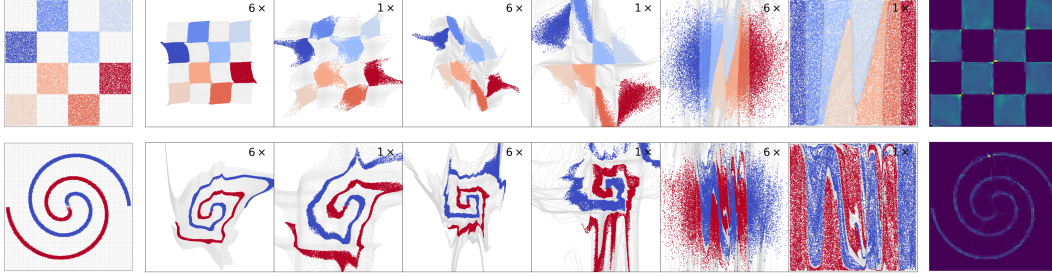


Figure 3. Illustration of diffeomorphic deformations on 2D toy problems. **Leftmost:** Samples from empirical distribution. **Middle:** Data distribution of intermediate mappings. The symbol “ $N \times$ ” in each grid denotes that the displayed domain is N times of the leftmost column. **Rightmost:** Density estimation by flow. The intermediate mappings reshape the data distribution by iteratively performing non-uniform stretching (expansive mapping) and compression (contractive mapping) on its domain.

dimensions, (ii) two consecutive coupling layers to capture the information of every dimension, and (iii) an elementwise activation with multimodal derivative to improve the non-linearity. Each block is parameterized by special structure to satisfy the Lipschitz constraint and initialized with blockwise volume-preserving strategy. A set of building blocks are then combined together with a multi-scale architecture.

4.1. Building Block

Linear layer via invertible convolution. We extend the invertible 1×1 convolution (Kingma & Dhariwal, 2018) to $k \times k$ convolution with k strides and k^2 times output channels compared to input. Such convolution is an invertible linear mapping if the weight of convolution is invertible, denoted as $f_{\text{conv}} : \mathbb{R}^d \rightarrow \mathbb{R}^d$. The map f_{conv} can be considered as a fused operation of squeezing and 1×1 convolution if $k > 1$. For instance, for a $h \times w \times c$ tensor, we have a $\frac{h}{k} \times \frac{w}{k} \times k^2 c$ output after the transform of f_{conv} . The determinant contributed by this convolution is equal to $hw/k^2 \det(w)$ in which w is its weight matrix. In our implementation, the weight is parameterized by a $k^2 c \times k^2 c$ square matrix and initialized as $\kappa \mathcal{I}$, where \mathcal{I} is an identity matrix, and κ a positive number to be discussed below.

Dual affine coupling layer. To let every dimension be transformed in an individual block, we stack two affine coupling layers (Dinh et al., 2017) together. More precisely, for a partition $\mathbf{x} = (\mathbf{x}_1, \mathbf{x}_2)$, $\mathbf{x}_1 \in \mathbb{R}^r$, $\mathbf{x}_2 \in \mathbb{R}^{d-r}$, $1 \leq r < d$, we define a layer of dual affine coupling $f_{\text{aff}} : \mathbb{R}^d \rightarrow \mathbb{R}^d$ by

$$\begin{aligned} \mathbf{y}_1 &= \mathbf{s}_1(\mathbf{x}_2) \odot \mathbf{x}_1 + \mathbf{t}_1(\mathbf{x}_2), \\ \mathbf{y}_2 &= \mathbf{s}_2(\mathbf{y}_1) \odot \mathbf{x}_2 + \mathbf{t}_2(\mathbf{y}_1), \end{aligned} \quad (14)$$

where $\mathbf{s}_1, \mathbf{t}_1 : \mathbb{R}^{d-r} \rightarrow \mathbb{R}^r$ and $\mathbf{s}_2, \mathbf{t}_2 : \mathbb{R}^r \rightarrow \mathbb{R}^{d-r}$ are maps parameterized by neural networks, \odot is the Hadamard product. In particular, it follows $\mathbf{s} > 0$ to ensure the invertibility of f_{aff} . The determinant $\det(J_{f_{\text{aff}}})$ is simply the product of every entries of \mathbf{s}_1 and \mathbf{s}_2 . To control the initialization and the output range of \mathbf{s} , the last layer of neural networks is

a linear layer followed by a mixture of M Mexican-hat-like activations:

$$\begin{aligned} \varphi_m(\mathbf{x}) &= w_m \phi(\mathbf{x}) + b_m, \\ \log \mathbf{s} &= \frac{1}{M} \sum_{m=1}^M (1 - \varphi_m^2) \exp\left(-\frac{\varphi_m^2}{2}\right), \end{aligned} \quad (15)$$

where ϕ is the pre-output of neural network, w_m the weight matrix initialized to 0, and b_m the bias term whose initialization follows the blockwise volume-preserving strategy. With this layer, \mathbf{s} is limited in the range (0.5, 3).

Monotonic rational-quadratic activation. To improve the multimodality of determinant mapping τ , we construct a monotonic and elementwise activation function $f_{\text{act}} : \mathbb{R} \rightarrow \mathbb{R}$ using rational-quadratic splines (Gregory & Delbourgo, 1982; Durkan et al., 2019). The function f_{act} is defined in the interval from $[x^{(0)}, x^{(I)}]$ to $[y^{(0)}, y^{(I)}]$, and is fully described by $3(I+1)$ parameters $\{(x^{(i)}, y^{(i)}, \alpha^{(i)})\}_{i=0}^I$ which satisfy $x^{(i)} < x^{(i+1)}$, $y^{(i)} < y^{(i+1)}$ and positive derivatives at the boundaries $\alpha^{(i)} > 0$. In each sub-interval (a.k.a. a bin) $[x^{(i)}, x^{(i+1)}]$, f_{act} is obtained by a rational-quadratic function. Let bin width $\Delta_x^{(i)} = x^{(i+1)} - x^{(i)}$, bin height $\Delta_y^{(i)} = y^{(i+1)} - y^{(i)}$, and bin ratio $\delta^{(i)} = \Delta_y^{(i)} / \Delta_x^{(i)}$, for a point $x \in [x^{(i)}, x^{(i+1)}]$, denote $\xi(x; i) = (x - x^{(i)}) / \Delta_x^{(i)}$ in which $0 \leq \xi \leq 1$, we have

$$f_{\text{act}}(\xi; i) = y^{(i)} + \frac{\Delta_y^{(i)} [\delta^{(i)} \xi^2 + \alpha^{(i)} \xi(1 - \xi)]}{\delta^{(i)} + \rho^{(i)} \xi(1 - \xi)}, \quad (16)$$

where $\rho^{(i)} = \alpha^{(i+1)} + \alpha^{(i)} - 2\delta^{(i)}$, for $i = 0, 1, \dots, I-1$. The function f_{act} is invertible with analytical inverse, and its first derivative is computationally tractable as

$$\frac{d}{dx} f_{\text{act}} = \frac{\gamma^{(i)} (\delta^{(i)})^2}{[\delta^{(i)} + \rho^{(i)} \xi(1 - \xi)]^2}, \quad (17)$$

where $\gamma^{(i)} = \alpha^{(i+1)} \xi^2 + 2\delta^{(i)} \xi(1 - \xi) + \alpha^{(i)} (1 - \xi)^2$. This derivative can be multimodal as $\max \sigma(df_{\text{act}}/dx) = I$,

when it can also be trivial as a constant if $\alpha^{(i)} = \delta^{(i)} = \beta$ is a same value for all i . In the case of the latter, $\rho^{(i)} = 0$ and f_{act} degenerates to a linear function with slope $df_{\text{act}}/dx = \gamma^{(i)} = \beta$.

The above three components are composed together as the building block of our model as $f_l = f_{\text{act}} \circ f_{\text{aff}} \circ f_{\text{conv}}$. To follow the principles discussed in Sec. 3, we wish the first two components $f_{\text{aff}} \circ f_{\text{conv}}$ to act as an expansive function with loose constraint. Here the constraint is flexible but important for training stability, and it is one of the reasons we limit the range of \mathbf{s} by Eq. (15). For f_{act} , we let it be contractive by limiting $\alpha^{(i)}, \delta^{(i)} \in (0, 1)$, which conditions are sufficient to let $df_{\text{act}}/dx \leq 1$ holds almost everywhere in its domain. To follow the strategy of blockwise volume-preserving initialization, we initialize every components as linear maps satisfying $\kappa(\mathbf{s})_j = 1/\beta$ by controlling the initialization of parameters κ, b_m and $(x^{(i)}, y^{(i)}, \alpha^{(i)})$. Thus f_l is initialized as a blockwise identity function with determinant:

$$\det(J_{f_{\text{conv}}}) \det(J_{f_{\text{aff}}}) = \frac{1}{\det(J_{f_{\text{act}}})} = \beta^{-d}, \quad (18)$$

in which β is a hyperparameter in $(0, 1]$, experically a narrower range $[0.5, 1]$ is advised.

4.2. Multi-scale Architecture

The multi-scale architecture introduced by Dinh et al. (2017) is a framework for the composition of multiple diffeomorphic transforms, where it factors out half of the dimensions at each scale. Formally, multi-scale architecture with two levels is a composition of diffeomorphisms as follows.

$$\begin{aligned} \mathbf{f} &= \mathbf{f}_2 \circ \mathbf{f}_1 : \mathbb{R}^d \rightarrow \mathbb{R}^d, \text{ where } \mathbf{f}_2 = (\text{id}, \mathbf{f}_3), \\ \text{id} : \mathbf{x} \in \mathbb{R}^r &\rightarrow \mathbf{x}, \mathbf{f}_3 : \mathbb{R}^{d-r} \rightarrow \mathbb{R}^{d-r}. \end{aligned} \quad (19)$$

There r is specified to $r = d/2$ in Dinh et al. (2017), while it can vary in range $[1, d]$. The function \mathbf{f}_3 could be another composition of diffeomorphisms in the same way, resulting in an architecture with multiple levels. An interesting property of multi-scale architecture is the importance ranking effect between dimensions, i.e., compared to the latent features generated by the identity mapping in \mathbf{f}_2 , the ones generated by the non-identity mapping \mathbf{f}_3 carry a different amount of information for reconstructing the input. This is a property shared with PPCA, known as dimensionality reduction. See our experiment in Sec. 6.3.

5. Related work

Related topics to our work include: (1) Tractability, in which the computational challenge of Jacobian determinant is concerned. (2) Expressivity, in which the construction of diffeomorphic mapping with restricted determinant is concerned. For these two topics, we refer to the surveys by Papamakarios et al. (2019) and Kobyzev et al. (2020).

Table 1. Density estimations of standard benchmarks in bits/dim (lower is better). The number in brackets is the number of parameters ($\times 10^6$). The results for QLF* are theoretical value calculated by equation (6).

MODEL	CIFAR10	IMAGENET 32	CELEBA 1024
REALNVP	3.49	4.28	-
GLOW	3.35 (44.0)	4.09	-
RQ-NSF	3.38 (11.8)	-	-
QLF*	2.01	1.75	-
OURS	3.37 (12.6)	4.03	0.64 (23.3)

Universality. As a complement of our work, Teshima et al. (2020) proves affine coupling flows (a case of QLF) are universal approximators in the sense of L^p norms, and Koehler et al. (2020) further shows the relation of universality with the depth of affine couplings. The universality for other invertible architectures is also explored by Zhang et al. (2020) (on continuous flows) and Kong & Chaudhuri (2020) (on matrix determinant lemma-based flows).

Flows via Optimal Transport. Optimal Transport (OT) provides a different measure of statistical distance from MLE, which encourages straight trajectories between two distributions (Onken et al., 2020) and in some sense penalizes unreasonable increase of volume. Recent work of Zhang et al. (2018), Finlay et al. (2020), Yang & Karniadakis (2020) and Onken et al. (2020) introduced OT into normalizing flows and found the training stability is improved. It would be interesting to further investigate whether QLF or other restricted flows have closed form formulas under the OT metric in future work.

6. Experiments

6.1. Density Estimation

To evaluate our proposed flow in density estimation, we train it on standard image benchmarks CIFAR10 (Krizhevsky & Hinton, 2009), downsampled 32×32 ImageNet (Rusakovsky et al., 2015) and CelebA-HQ 1024×1024 (Karras et al., 2017). The results in Table. 1 demonstrate that the performance of our model is similar to RQ-NSF on CIFAR10, and slightly better than Glow on ImageNet 32×32 . Benefit from the multimodal activation, compared to Glow, significantly less parameters is required to achieve the same score. In addition, our model is scalable to CelebA-HQ 1024×1024 , while the others are absent in this dataset due to numerical issues or memory limitation. To the best of our knowledge, it is the first flow-based model in the literature that can train on this scale. In particular, the values of QLF show the gap between theoretical and experimental optima, providing a useful guidance for model design.

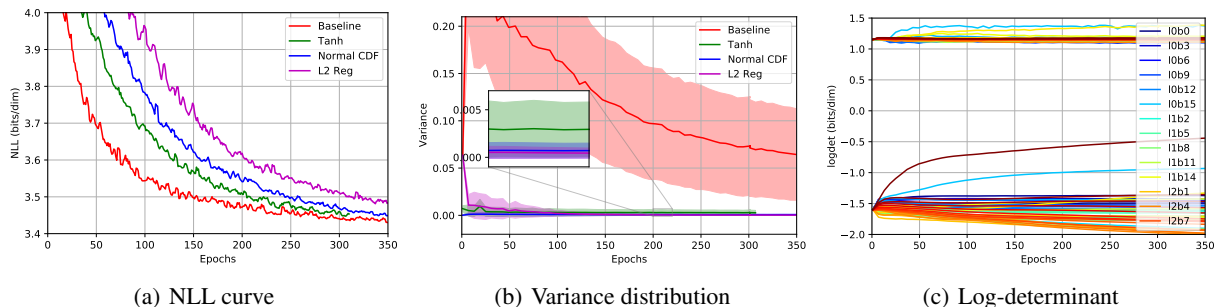


Figure 4. Training curves on CIFAR10. (a) Negative log-likelihood (NLL) curves. (b) The distribution of the variance for all intermediate mappings. (c) The log-determinant of each intermediate mapping, an expansive layer followed by a contractive layer.

6.2. Effect of Lipschitzness

We explore the effect of Lipschitzness on CIFAR10. In Fig. 4, the baseline is our proposed flow. As a comparison, contractive activations Tanh and normal CDF are inserted between f_{aff} and f_{act} , and L_2 transport cost is applied to the output of f_{act} , respectively. These added activations or regularity have tighter constraint than the baseline. And they lead to slower convergence and worse NLL estimation (Fig. 4 (a)). For a model having worse NLL performance, it also has smaller averaged variance over all intermediate maps (Fig. 4 (b)). In contrast, the model without any constraint on f_{aff} and f_{act} converges faster and has higher variance at the beginning of training, but soon collapses due to the gradient problems, thus no training curve is displayed. This result validates the relationship between Lipschitzness of f , boundedness of τ , and variance change by f discussed in Sec. 2.

6.3. Multi-scale Architecture for Dimensionality Reduction

In Fig. 5, we use an 8 levels model pretrained on CelebA-HQ 1024×1024 to obtain the latent variables of real image, then partially resample these variables from a noise distribution, and finally decode the perturbed variables to get the reconstruction image. The results show that the latent variables in a higher level are more informative for the reconstruction. This can be explained as follows. Group the latent variables $\mathbf{z} = (z_1, z_2, \dots)$ by the corresponding level order, and consider the determinant map on generation direction $\pi(\mathbf{z}) = \tau(g(\mathbf{z})) : \mathbf{z} \mapsto |\det J_g(\mathbf{z})|$ as a hypersurface embedded in \mathbb{R}^{d+1} , when varying the dimensions in the i -th level but fixing the others, a new hypersurface $\pi_i : \mathbf{y} \mapsto \pi(\mathbf{z}_{i-1}, \mathbf{y}, \mathbf{z}_{i+1})$ in the subspace is generated. Due to the careful design of multi-scale architecture, the function π_i with lower level i has less layer thus is less complex. This results in that the hypersurface π along the directions of the i -th group of dimensions are smoother, which dimensions containing less information about the

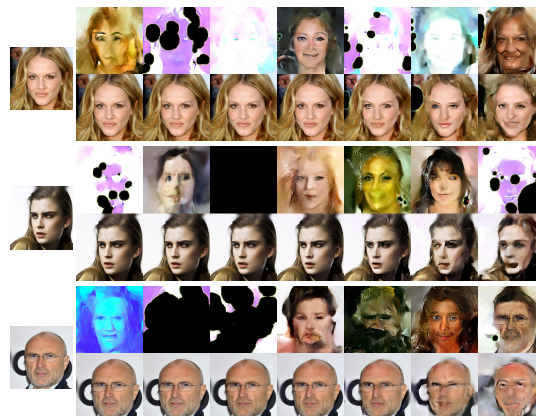


Figure 5. Perturbations of latent variables. The leftmost column represents the original image, while the others are reconstructions. More specifically, the reconstruction in the k -th column ($k \geq 1$) and the first row relative to each real image is obtained by storing the latent variables in the first k levels and resampling the others, while the second row resampling the first k levels and storing the others. Latent variables in an earlier layer have smaller level order. The results indicate the latent variables in higher levels contain more information about the data.

dataset. This property is useful for dimensionality reduction and data compression, specifically for the scenario of data transmission by extracting latent variables in high levels and reconstructing at the remote.

7. Conclusion

This work demonstrates the uniqueness of Jacobian determinant mapping through Radon-Nikodym theorem, and shows the closed form exists for flows in the form of QLF. For the training of flows, the convergence condition is given. In addition, a new flow is proposed and its improved stability and scalability are validated by numerical experiments. Normalizing flow is essentially a nonlinear extension of PPCA, so it has the potential for applications where PPCA is applicable, such as dimensionality reduction and data reconstruction.

References

- Behrmann, J., Grathwohl, W., Chen, Ricky T. Q. and Duvenaud, D., and Jacobsen, J. Invertible residual networks. In *International Conference on Machine Learning*, 2019.
- Chen, R. T. Q., Behrmann, J., Duvenaud, D., and Jacobsen, J. Residual flows for invertible generative modeling. In *Advances in Neural Information Processing Systems*, pp. 9916–9926, 2019.
- Chen, T., Xu, B., Zhang, C., and Guestrin, C. Training deep nets with sublinear memory cost. *arXiv preprint arXiv:1604.06174*, 2016.
- Dinh, L., Krueger, D., and Bengio, Y. Nice: Non-linear independent components estimation. *arXiv preprint arXiv:1410.8516*, 2014.
- Dinh, L., Sohl-Dickstein, J., and Bengio, S. Density estimation using real nvp. *International Conference on Learning Representations*, 2017.
- Dupont, E., Doucet, A., and Teh, Y. W. Augmented neural odes. *arXiv preprint arXiv:1904.01681*, 2019.
- Durkan, C., Bekasov, A., Murray, I., and Papamakarios, G. Neural spline flows. *Advances in Neural Information Processing Systems*, 2019.
- Finlay, C., Jacobsen, J.-H., Nurbekyan, L., and Oberman, A. How to train your neural ode: the world of jacobian and kinetic regularization. In *International Conference on Machine Learning*, pp. 3154–3164, 2020.
- Grathwohl, W., Chen, R. T. Q., Bettencourt, J., Sutskever, I., and Duvenaud, D. Ffjord: Free-form continuous dynamics for scalable reversible generative models. *International Conference on Learning Representations*, 2019.
- Gregory, J. and Delbourgo, R. Piecewise rational quadratic interpolation to monotonic data. *IMA Journal of Numerical Analysis*, 2(2):123–130, 1982.
- He, K., Zhang, X., Ren, S., and Sun, J. Deep residual learning for image recognition. In *Proceedings of the IEEE conference on computer vision and pattern recognition*, pp. 770–778, 2016.
- Ho, J., Chen, X., Srinivas, A., Duan, Y., and Abbeel, P. Flow++: Improving flow-based generative models with variational dequantization and architecture design. In *International Conference on Machine Learning*, 2019.
- Hu, J., Shen, L., and Sun, G. Squeeze-and-excitation networks. In *Proceedings of the IEEE conference on computer vision and pattern recognition*, pp. 7132–7141, 2018.
- Huang, C., Dinh, L., and Courville, A. Augmented normalizing flows: Bridging the gap between generative flows and latent variable models. *arXiv preprint arXiv:2002.07101*, 2020a.
- Huang, C., Dinh, L., and Courville, A. Solving ode with universal flows: Approximation theory for flow-based models. In *ICLR 2020 Workshop on Integration of Deep Neural Models and Differential Equations*, 2020b.
- Karras, T., Aila, T., Laine, S., and Lehtinen, J. Progressive growing of gans for improved quality, stability, and variation. *arXiv preprint arXiv:1710.10196*, 2017.
- Kingma, D. P. and Ba, J. Adam: A method for stochastic optimization. *arXiv preprint arXiv:1412.6980*, 2014.
- Kingma, D. P. and Dhariwal, P. Glow: Generative flow with invertible 1x1 convolutions. In *Advances in Neural Information Processing Systems*, pp. 10236–10245, 2018.
- Kingma, D. P., Salimans, T., Jozefowicz, R., Chen, X., Sutskever, I., and Welling, M. Improved variational inference with inverse autoregressive flow. In *Advances in neural information processing systems*, pp. 4743–4751, 2016.
- Kobyzev, I., Prince, S., and Brubaker, M. Normalizing flows: An introduction and review of current methods. *IEEE Transactions on Pattern Analysis and Machine Intelligence*, 2020.
- Koehler, F., Mehta, V., and Risteski, A. Representational aspects of depth and conditioning in normalizing flows. *arXiv preprint arXiv:2010.01155*, 2020.
- Kong, Z. and Chaudhuri, K. The expressive power of a class of normalizing flow models. *arXiv preprint arXiv:2006.00392*, 2020.
- Krizhevsky, A. and Hinton, G. Learning multiple layers of features from tiny images. Technical report, Citeseer, 2009.
- Liao, H., He, J., and Shu, K. Generative model with dynamic linear flow. *IEEE Access*, 7:150175–150183, 2019.
- Meng, C., Song, Y., Song, J., and Ermon, S. Gaussianization flows. In *International Conference on Artificial Intelligence and Statistics*, pp. 4336–4345. PMLR, 2020.
- Miyato, T., Kataoka, T., Koyama, M., and Yoshida, Y. Spectral normalization for generative adversarial networks. *arXiv preprint arXiv:1802.05957*, 2018.
- Müller, T., McWilliams, B., Rousselle, F., Gross, M., and Novák, J. Neural importance sampling. *ACM Transactions on Graphics*, 38(5):1–19, 2019.

- Onken, D., Fung, S. W., Li, X., and Ruthotto, L. Ot-flow: Fast and accurate continuous normalizing flows via optimal transport. *arXiv preprint arXiv:2006.00104*, 2020.
- Papamakarios, G., Pavlakou, T., and Murray, I. Masked autoregressive flow for density estimation. In *Advances in Neural Information Processing Systems*, pp. 2338–2347, 2017.
- Papamakarios, G., Nalisnick, E., Rezende, D. J., Mohamed, S., and Lakshminarayanan, B. Normalizing flows for probabilistic modeling and inference. *arXiv preprint arXiv:1912.02762*, 2019.
- Rezende, D. and Mohamed, S. Variational inference with normalizing flows. In *Proceedings of the 32nd International Conference on Machine Learning*, volume 37, pp. 1530–1538, 07–09 Jul 2015.
- Rudin, W. *Real and complex analysis, 3rd edition*. McGraw-Hill, New York, 1987.
- Russakovsky, O., Deng, J., Su, H., Krause, J., Satheesh, S., Ma, S., Huang, Z., Karpathy, A., Khosla, A., Bernstein, M., et al. Imagenet large scale visual recognition challenge. *International journal of computer vision*, 115(3): 211–252, 2015.
- Teshima, T., Ishikawa, I., Tojo, K., Oono, K., Ikeda, M., and Sugiyama, M. Coupling-based invertible neural networks are universal diffeomorphism approximators. In *Advances in Neural Information Processing Systems*, volume 33, pp. 3359–3370, 2020.
- Tipping, M. E. and Bishop, C. M. Probabilistic principal component analysis. *Journal of the Royal Statistical Society, Series B*, 61(3):611–622, 1999.
- van den Berg, R., Hasenclever, L., Tomczak, J., and Welling, M. Sylvester normalizing flows for variational inference. In *proceedings of the Conference on Uncertainty in Artificial Intelligence*, 2018.
- Yang, L. and Karniadakis, G. E. Potential flow generator with l_2 optimal transport regularity for generative models. *IEEE Transactions on Neural Networks and Learning Systems*, 2020.
- Zhang, H., Gao, X., Unterman, J., and Arodz, T. Approximation capabilities of neural ODEs and invertible residual networks. In *Proceedings of the 37th International Conference on Machine Learning*, volume 119, pp. 11086–11095, 13–18 Jul 2020.
- Zhang, L., Wang, L., et al. Monge-ampere flow for generative modeling. *arXiv preprint arXiv:1809.10188*, 2018.

A. Quasi-Linear Flow

A.1. The Stationary Point of QLF

Suppose the determinant of \mathbf{W} is positive. To obtain the stationary point of QLF, we can calculate the gradient of Eq. (5) with respect to \mathbf{W} at point \mathbf{x} :

$$\frac{\partial \mathcal{L}}{\partial \mathbf{W}} = -\mathbf{W}\mathbf{S}^T + (\mathbf{W}^{-1})^T \quad (20)$$

Note that \mathbf{W} is invertible. At the stationary point, $\mathbf{S} = \mathbf{W}^{-1}(\mathbf{W}^{-1})^T$. Since \mathbf{S} is symmetric, applying eigendecomposition, we have $\mathbf{S} = \mathbf{V}\Lambda\mathbf{V}^T$, in which \mathbf{V} is orthogonal whose columns are the eigenvectors of \mathbf{S} and Λ is diagonal with the corresponding eigenvalues. Therefore, there is a solution when $\mathbf{W} = \mathbf{U}\Lambda^{-1/2}\mathbf{V}^T$ with \mathbf{U} being an arbitrary orthogonal matrix.

A.2. Comparison with PPCA

For the case of \mathbf{W} and \mathbf{b} being independent of \mathbf{x} , Eq. (5) can be rewritten as

$$\mathcal{L} = -\frac{1}{2} \left\{ d \log 2\pi + \text{tr}(\mathbf{M}\mathbf{S}') + \log |\det(\mathbf{M}^{-1})| \right\}, \quad (21)$$

in which $\mathbf{S}' = \mathbb{E}_{p_{\mathbf{x}}}[\mathbf{x}\mathbf{x}^T]$ is the sample covariance matrix of the observations (supposing \mathbf{x} is zero-mean). In this case, it can be shown that Eq. (21) is maximized when $\mathbf{W} = \mathbf{U}\Lambda^{-1/2}\mathbf{V}^T$, where \mathbf{V} and Λ are the eigenvectors and eigenvalues of \mathbf{S}' respectively. Restricting all the smallest $d - r$ eigenvalues to be σ^2 and separating them from Λ , then the corresponding latent variables form the noise term $\epsilon \sim \mathbb{N}(0, \sigma^2 I)$ in the original PPCA (Tipping & Bishop, 1999), while the other r terms are the principal components.

B. Proofs

Proof. Inequality (8)

The function \mathbf{f} is assumed to be differentiable and K -Lipschitz continuous. Therefore, by definition, for every normalized eigenvector \mathbf{e}_i and $\varepsilon > 0$, there exists $\delta > 0$ such that if $h < \delta$ we have

$$\left| \frac{\|\mathbf{f}(\mathbf{x} + h\mathbf{e}_i) - \mathbf{f}(\mathbf{x})\|}{h} - \|J_{\mathbf{f}}(\mathbf{x})\mathbf{e}_i\| \right| < \varepsilon. \quad (22)$$

Therefore

$$\|J_{\mathbf{f}}(\mathbf{x})\mathbf{e}_i\| < \frac{\|\mathbf{f}(\mathbf{x} + h\mathbf{e}_i) - \mathbf{f}(\mathbf{x})\|}{h} + \varepsilon < K + \varepsilon. \quad (23)$$

Since this holds for every ε , we have $\|J_{\mathbf{f}}(\mathbf{x})\mathbf{e}_i\| < K$. By induced matrix norm $\|J_{\mathbf{f}}(\mathbf{x})\| := \sup_{\|\mathbf{e}_i\|=1} \|J_{\mathbf{f}}(\mathbf{x})\mathbf{e}_i\|$, we have

$$\|J_{\mathbf{f}}(\mathbf{x})\mathbf{e}_i\| \leq \|J_{\mathbf{f}}(\mathbf{x})\| \leq K, \quad (24)$$

Furthermore, by Hadamard's inequality, $|\det(J_{\mathbf{f}}(\mathbf{x}))| \leq \prod_{i=1}^d \|J_{\mathbf{f}}(\mathbf{x})\mathbf{e}_i\|$. Hence the inequality (8) gets proven. \square

Proof. Proposition 1

For $l \in \{1, 2, \dots, L\}$, assume $\|\boldsymbol{\theta}_l\|$ is bounded from above, i.e., there exists finite $C > 0$ such that $\|\boldsymbol{\theta}_l\| \leq C$ for all $\mathbf{x} \in \mathbf{X}$. By Eq. (13), we have

$$\overbrace{\frac{\partial \mathbf{h}_{l+1}}{\partial \boldsymbol{\theta}_l}}^{\alpha} \cdot \prod_{\substack{j=l+1 \\ j \neq i}}^L \|J_{\mathbf{f}_j}\| \cdot \|J_{\mathbf{f}_i}\| + o \leq C, \text{ for } l+1 \leq i \leq L. \quad (25)$$

Note o is non-negative, therefore

$$\alpha \|J_{\mathbf{f}_i}\| \leq C. \quad (26)$$

Now consider the term α , since \mathbf{f}_l is invertible for all l , we have $0 < |\det(J_{\mathbf{f}_j})|^{1/d} \leq \|J_{\mathbf{f}_j}\|$. Moreover, it is reasonable to assume there are finite points such that $\|\frac{\partial \mathbf{h}_{l+1}}{\partial \boldsymbol{\theta}_l}\| = 0$, so $\alpha > 0$ holds almost everywhere. For the case $\alpha > 0$, if $\|J_{\mathbf{f}_i}\|$ is

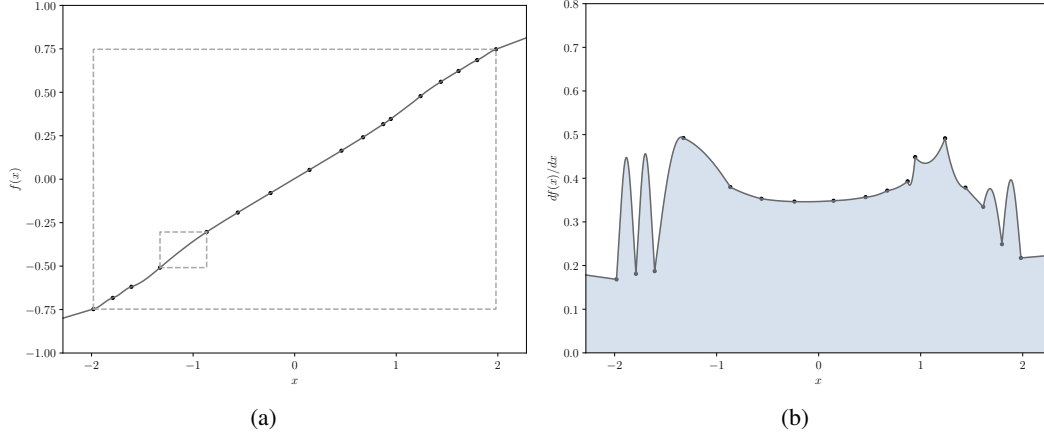


Figure 6. An example of monotonic rational-quadratic activation (a) and its derivative curve (b).

unbounded, i.e., there exists a point \mathbf{x} and a real number $K_i > 0$ such that $\alpha \|J_{f_i}(\mathbf{x})\| > \alpha K_i$. It holds for every K_i , hence we can always find a K_i such that $\alpha \|J_{f_i}(\mathbf{x})\| > C$. However, this contradicts Eq. (26), thus $\|J_{f_i}\|$ must be bounded (by finite $K_i > 0$). Easily, $\sum_l \log |\det(J_{f_l})| \leq \sum_l d \log K_l = d \log \prod_l K_l$ is also true. \square

C. Experimental Details

Neural Networks. For the implementation of neural networks in dual affine coupling layers, we use a residual network (ResNet; He et al. 2016) for CIFAR10 and Imagenet 32×32 , and a simple convolutional network (ConvNet) for CelebA-HQ 1024×1024 . Concretely, in ResNet, a 3×3 convolution layer is followed by one residual bottleneck block with 3 convolution layers (kernel size of $1 \times 1, 3 \times 3, 1 \times 1$ respectively) gated by channel-wise attention (Hu et al., 2018), followed by two 1×1 convolution layers between which another channel-wise attention is inserted. In ConvNet, due to computational resource constrains, three convolutional layers with kernel size of $3 \times 3, 1 \times 1, 3 \times 3$ respectively are used. The number of hidden units is 128 in ResNet, and 256 in ConvNet.

Rational-quadratic Activation. In order to restrict the range of derivative, we have a different implementation from Durkan et al. (2019). In our implementation, the knots $\{x^{(i)}, y^{(i)}, \alpha^{(i)}\}_{i=0}^I$ is parameterized by vectors $\theta_x, \theta_y, \theta_a \in \mathbb{R}^{I+1}$ respectively. The ratio of height and width $\delta^{(i)}$ in each bin (the inner box in Fig. 6 (a)) is strictly limited in range $[0, 1]$ by

$$\bar{b}_x = \text{softmax}(\theta_x), \quad (27)$$

$$\bar{b}_y = \text{sigmoid}(\theta_y) \cdot \bar{b}_x, \quad (28)$$

$$x^{(i)} = (2 \times \text{cumsum}(\bar{b}_x)_i - 1)w, \quad (29)$$

$$b_y = \text{cumsum}(\bar{b}_y), \quad (30)$$

$$y^{(i)} = (2 \times (b_y)_i - \max(b_y))w, \quad (31)$$

where cumsum is the cumulative sum of its inputs, and w is a learnable variable that controls the width and position of the outer box in Fig. 6 (a). The derivative at each knots is also limited in range $[0, 1]$ by

$$\alpha^{(i)} = \text{sigmoid}(\theta_a)_i. \quad (32)$$

By this way, the derivative of activation is less than one almost everywhere (Fig. 6 (b)). For the region out of the outer box, it is also treated as a bin. For instance, the region (w, ∞) is a bin whose right boundary is represented by a relative large number (e.g. 1×10^5) and the parameters of right boundary are fixed during training. In our experiments, the number of bins is $I = 16$.

Multi-scale Architecture. For datasets CIFAR10 and ImageNet 32×32 , the model has 3 levels with 16 blocks per level, and half of the dimensions is splitted out at each level. For CelebA-HQ 1024×1024 , the model has 8 levels with 12 blocks

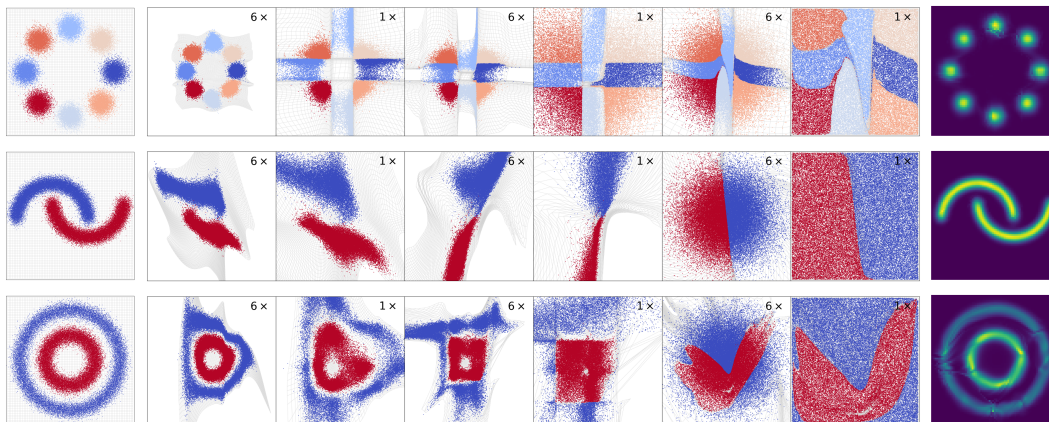


Figure 7. Illustration of diffeomorphic deformations on 2D toy problems. **Leftmost:** Samples from empirical distribution. **Middle:** Data distribution of intermediate mappings in the order of layer number. The symbol “ $N \times$ ” in each grid denotes that the displayed domain is N times of the leftmost column. **Rightmost:** Density estimation by flow. The intermediate mappings reshape the data distribution by iteratively performing non-uniform stretching (expansive mapping) and compression (contractive mapping) on its domain.

per level, and 3/4 of the dimensions is splitted out at each level.

Optimization details. We use Adamax optimizer (Kingma & Ba, 2014) with default β_1 and β_2 . And learning rate is set to 0.01 and exponentially decreases to 0.001 with 1×10^3 decay steps and 0.98 decay rate. We use the gradient checkpointing trick (Chen et al., 2016) to improve the memory utilization. Batch size is set to 1024 for CIFAR10 and ImageNet 32×32 , and 4 for CelebA-HQ 1024×1024 . The preprocessing and division of datasets follow the method used in Kingma & Dhariwal (2018).

D. Extra Samples

Additional samples on 2D toy problems and generated samples from CelebA-HQ 1024×1024 are shown in Fig. 7 and Fig. 8, respectively.

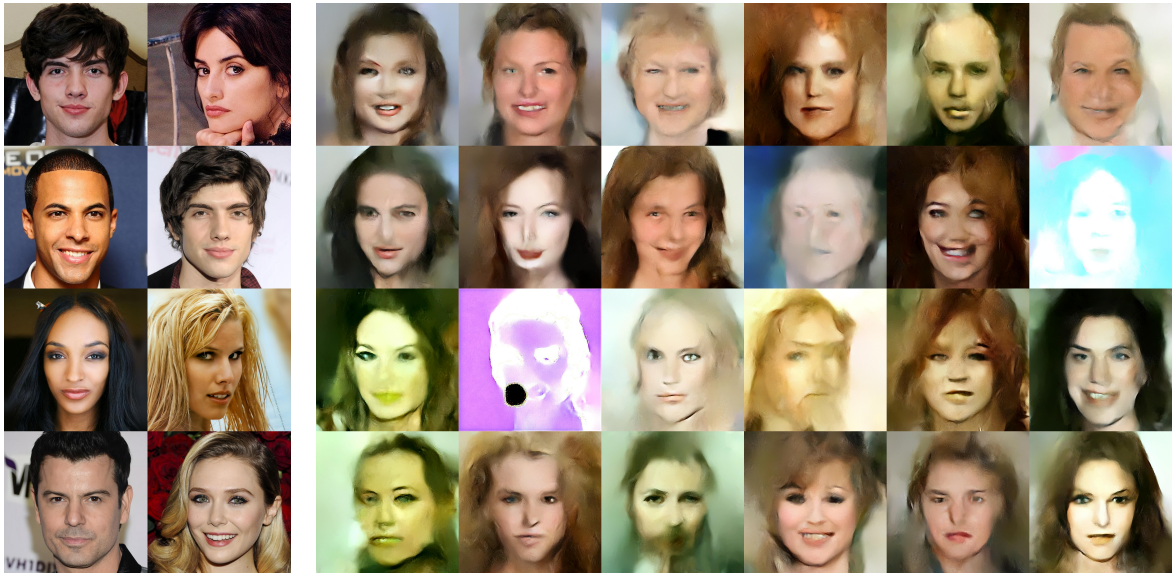


Figure 8. **Left:** Real samples. **Right:** Randomly generated samples from 5bit CelebA-HQ 1024×1024 , with temperature 0.9.